Clear Underwater Vision

Yoav Y. Schechner and Nir Karpel
Dept. of Electrical Engineering
Technion - Israel Inst. Technology
Haifa 32000, ISRAEL
yoav@ee.technion.ac.il , karpeln@tx.technion.ac.il

Abstract

Underwater imaging is important for scientific research and technology, as well as for popular activities. We present a computer vision approach which easily removes degradation effects in underwater vision. We analyze the physical effects of visibility degradation. We show that the main degradation effects can be associated with partial polarization of light. We therefore present an algorithm which inverts the image formation process, to recover a good visibility image of the object. The algorithm is based on a couple of images taken through a polarizer at different orientations. As a by product, a distance map of the scene is derived as well. We successfully used our approach when experimenting in the sea using a system we built. We obtained great improvement of scene contrast and color correction, and nearly doubled the underwater visibility range.

1 Underwater Vision

Underwater imaging is widely used in scientific research and technology. Computer vision methods are being used in this mode of imaging for various applications [3, 32, 36], such as mine detection, inspection of underwater power and telecommunication cables, pipelines [10], nuclear reactors, and columns of offshore platforms [10]. Underwater computer vision is commercially used to help swimming pool life guards [18]. As in conventional computer vision, algorithms are sought for navigation and control [37] of submerged robots. In addition, underwater imaging is used for research in marine biology [2, 7, 13, 36], archaeology [15] and mapping [37]. Moreover, underwater photography [34] is becoming more accessible to the wider public.

Underwater vision is plagued by poor visibility conditions [11, 14, 32, 36]. According to Ref. [10], most computer vision methods (e.g., those based on stereo triangulation or on structure from motion) cannot be employed directly underwater. This is due to the particularly challenging environmental conditions, which complicate image matching and analysis. It is therefore important to alleviate these visibility problems. What makes underwater imaging so problematic? To understand the challenge, consider Fig. 1, which shows an archaeological site ≈ 2.5m under the water surface. It is easy to see that visibility degradation effects

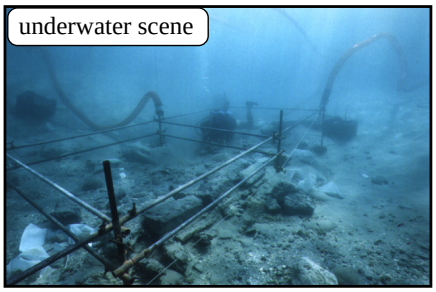

Figure 1. An underwater Mediterranean archaeological site. The visibility and colors quickly degrade as a function of distance. Courtesy of Yaakov Kahanov.

vary as distances to the objects increase [14]. Since objects in the field of view are at different distances from the camera, the *causes* for image degradation are spatially varying. This situation is analogous to open-air vision in bad weather (fog or haze), described in Refs. [5, 23, 24, 26]. Contrary to this fact, traditional image enhancement tools, e.g., high pass filtering and histogram equalization are typically spatially invariant. Since they do not model the spatially varying distance dependencies, traditional methods are of limited utility in countering visibility problems, as has been demonstrated in experiments [24, 26].

In this work we develop a physics-based approach for recovery of visibility when imaging underwater scenes in natural illumination. Since it is based on the image formation model, the method automatically accounts for dependencies on object distance, and estimates a distance map of the scene as a by-product. The approach relies on raw images taken through different states of a *polarizing filter*.[1] These raw images have slight photometric differences. These differences serve as initial cues for an algorithm that factors out turbidity effects. Interestingly, note that marine animals use polarization for improved vision [7, 27, 35, 36].

Some methods improve underwater visibility by using specialized active radiation hardware [11, 14, 19]. In contrast, we deal with a passive computer vision approach, exploiting natural illumination. Other prior methods are based either on a simple subtraction of images that are differ-

[1] Polarization has been used in various computer vision algorithms dealing with reflections [9, 25, 28, 30, 36]. These methods evolved along with developments of polarimetric imaging devices [8, 36].

ently polarization filtered [8, 11], or display the degree of polarization (DOP) [27, 32]. They assume that polarization is associated with the object radiation, rather than the causes which degrade this signal. However, this assumption becomes invalid as distances increase [22]. Our approach is based on a contrary fact [17, 21]: in natural illumination, underwater polarization is associated with the prime visibility disturbance which we wish to delete (termed *backscatter*). Our approach inverts the physical model, thus the recovered image is similar to clear visibility appearance, contrary to methods which merely attempt image enhancement [8, 11, 27, 32].

To demonstrate the approach, we built an underwater polarization imaging system. We describe the considerations for selecting the system components. We used the approach by experimenting in the sea. Significant improvements of contrast and color are obtained. The recovered range map indicates that the visibility range has been approximately doubled, thanks to the approach.

2 Modelling the Image Formation

Imaging conditions underwater are quite different than in the open air. In the open air, on clear days the sun is a dominant source, which lies low in mornings and afternoons. It lies low throughout the day in high geographic latitudes. Alternatively, on a cloudy day natural lighting may come from the entire hemisphere. In contrast, underwater natural lighting comes from a limited cone *above* the scene, as depicted in Fig. 2. This phenomenon is caused by refraction of the illuminating rays through the water surface, and is termed the *optical manhole* or *Snell's window* [6, 13]. Once in the water, the natural illumination undergoes a strong color-dependent attenuation. As a result, it typically becomes predominantly green-blue [34], resulting in images having this hue. Then, part of this light interacts the viewed scene.

As depicted in Fig. 3, when imaging underwater we sense two sources. The first source is the scene object at distance z, whose radiance is attenuated by absorption and scattering in the water. It is also somewhat blurred. The image corresponding to this degraded source is the *signal*. The second source is the ambient illumination. Part of that light is scattered towards the camera by the particles in the water. It is termed *backscattered light* [14, 20, 21]. This section describes each of these components.

2.1 The Signal

2.1.1 Direct Transmission

The signal is composed of two components, termed *direct transmission* and *forward scattering* [14, 20, 21]. As a light ray progresses from the object towards the camera, part of its energy is lost due to scattering and absorption. The fraction reaching the camera is the direct transmission[2]

[2]There is a proportion factor between the scene radiance and image irradiance that depends on the imaging system, but does not depend on the medium and its characteristics. We thus leave this factor out.

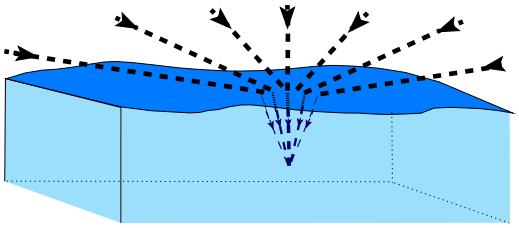

Figure 2. The optical manhole. Due to refraction at the water surface, natural underwater lighting comes from above.

$$D = L_{\text{object}} e^{-\eta z} \quad , \tag{1}$$

where η is the attenuation coefficient. Here L_{object} is the object radiance we would have sensed, had there been no scattering and absorption along the line of sight (LOS).

The attenuation coefficient is given by $\eta = \alpha + \beta$, where α is the absorption coefficient and β is the total scattering coefficient of the water. The scattering coefficient β expresses the ability of an infinitesimal water volume to scatter flux in all directions. Integrating over all solid angles $\vec{\Theta}$,

$$\beta = \int_{\vec{\Theta}} \beta(\vec{\Theta}) d\Omega = 2\pi \int_0^{\pi} \beta(\theta) \sin(\theta)\, d\theta \quad , \tag{2}$$

where θ is the scattering angle relative to the propagation direction, and $\beta(\theta)$ is the angular scattering coefficient. The variables $\alpha, \beta(\theta), \eta$ and L_{object} are all functions of the wavelength λ.

2.1.2 Forward Scattering

The forward scattering component is similar to the direct transmission. However, it represents light scattered forward at small angles relative to LOS. This creates image blur given by the convolution

$$F = D * g_z \quad , \tag{3}$$

where D is given by Eq. (1) and g_z is a point spread function (PSF). The PSF is parameterized by the distance z, since the farther the object, the wider the support of the blur kernel.

There are several models in the literature for the form of the underwater PSF [20, 33]. Since the PSF depends on the hydrsols suspended in the water, the models are typically parameterized by various empirical constants. For example, the model in Refs. [14, 20] is of the form

$$g_z = \left(e^{-\gamma z} - e^{-\eta z}\right) \mathcal{F}^{-1}\{G_z\} \text{ where } G_z = e^{-K z \omega} \tag{4}$$

while $K > 0$ and γ are empirical constants, $\mathcal{F}^{-1}$ is the inverse Fourier transform, and ω is the spatial frequency in the image plane. The filter G_z is low pass. Its effective frequency "width" is inversely proportional to z. This expresses the increase of spatial blur for distant objects. The constant γ is limited to $|\gamma| \leq \eta$ [20]. Note that the models of the PSF obtained empirically and through numerical simulations [20, 33] do not conserve energy as light propagates in z. This is clearly the case in Eq. (4). Thus forward scattering is a blurred and attenuated version D.

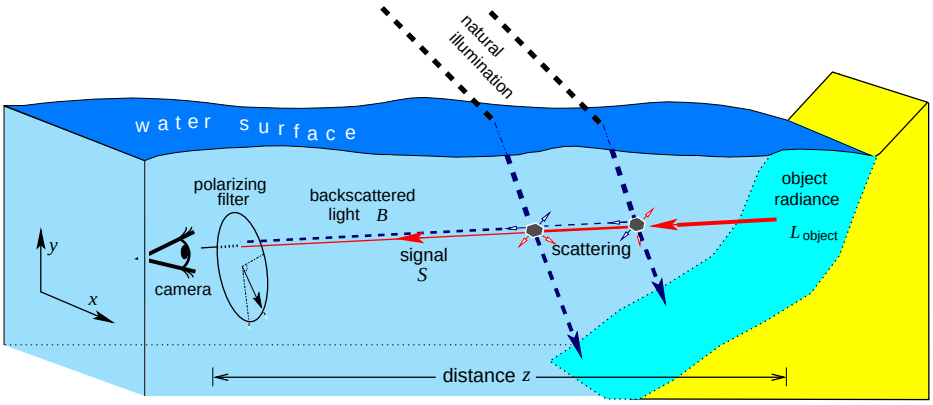

Figure 3. Underwater imaging of a scene, e.g., a reef, through a polarizing filter. [Dashed rays] Light coming from a source is backscattered towards the camera by particles in the water. The backscatter increases with the distance z to the object. [Solid ray] Light emanating from the object is attenuated and somewhat blurred as z increases, leading to the signal S. Without scattering and absorption along the line of sight (LOS), the object radiance would have been L_{object}.

Accounting for both the direct transmission (1) and the forward scattering (3), we define the *signal* as

$$S = D + F \quad . \tag{5}$$

We define an *effective* object radiance $L_{\text{object}}^{\text{effective}}$ as

$$L_{\text{object}}^{\text{effective}} = L_{\text{object}} + L_{\text{object}} * g_z \quad . \tag{6}$$

It is a somewhat blurred version of L_{object}. From Eqs. (1,3,5), the signal is

$$S = e^{-\eta z}\, L_{\text{object}}^{\text{effective}} \quad . \tag{7}$$

2.2 Backscattered Light

Backscatter does not originate from the object on the LOS. Rather, light coming from ambient illumination sources is scattered into the LOS and towards the camera by suspended particles (Fig. 3). Before integrating all the contributions to the illumination of the LOS, let us first analyze the effect of a single distant source. The source illuminates the particles on the LOS from direction $\vec{r} = (\theta, \varphi)$ relative to the LOS, with intensity I^{source}. Following Refs. [14, 20], the contribution of this source to the backscatter is

$$B\left(\vec{r}\right) = \int_0^z \beta\left(\theta\right) I^{\text{source}}\left(\vec{r}\right) e^{-\eta l} [1 - f/(l + l_0)]^2 dl \tag{8}$$

where f is the focal length of the camera and l_0 is the distance between the lens and the underwater housing window. This integral accounts for scattering into the LOS at some distance l, followed by attenuation until reaching the camera. It also accounts for geometric projection of the irradiance on the detector, via the ratio $f/(l + l_0)$.

The exponent in Eq. (8) sets a *typical* attenuation distance of $l \sim \eta^{-1}$ in the water. We exploit this observation to make a practical simplification of Eq. (8): typically $f/(\eta^{-1} + l_0) \ll 1$, making the effect of the $f/(l + l_0)$ term very small. Consider typical ranges of values as $\eta^{-1} \in [3m, 10m]$ (according to [21]), $f \in [20mm, 50mm]$, $l_0 \approx 80mm$, and object distance in the order of meters. We assessed the integrals numerically. It can be shown that to an accuracy of 99%, we can write Eq. (8) as

$$B(\vec{r}) \approx \kappa(f)\beta(\theta) I^{\text{source}}(\vec{r}) \int_0^z e^{-\eta l} dl \tag{9}$$

where $\kappa(f)$ is a constant parameterized by the focal length of the camera lens. A focal length of $f = 20mm$ corresponds to $\kappa = 1.06$. Eq. (9) is solved as

$$B(\vec{r}) = B_\infty(\vec{r}) \left(1 - e^{-\eta z}\right) \quad , \tag{10}$$

where

$$B_\infty(\vec{r}) \equiv \kappa I^{\text{source}}(\vec{r}) \beta(\theta)/\eta \tag{11}$$

is the backscatter in a LOS which extends to infinity in the water. Summing up the contribution from light sources at all directions, the total backscatter is

$$B = \int_{\vec{r}} B(\vec{r}) d(\vec{r}) = \; B_\infty \left(1 - e^{-\eta z}\right) \quad , \tag{12}$$

where

$$B_\infty \equiv \int_{\vec{r}} B_\infty(\vec{r}) d\vec{r} \tag{13}$$

is a scalar which depends on λ.

It is simple to show that a similar expression is obtained when generalizing to non-distant light sources (as particles in the water volume). This happens under the assumption that lighting does not vary along the LOS, or that such variations are practically integrated out. We believe that this is a reasonable assumption when imaging approximately horizontally. The reason is that natural underwater light comes from a limited light cone directly above [6, 13] (See Fig. 2), and is thus typically unobscured along the LOS.

We now discuss the significance of backscatter in image degradation. The total image irradiance is

$$I^{\text{total}} = S + B = e^{-\eta z}\, L_{\text{object}}^{\text{effective}} + B \quad . \tag{14}$$

To gain intuition about the contribution of each component, we performed a simulation of underwater imaging, whose

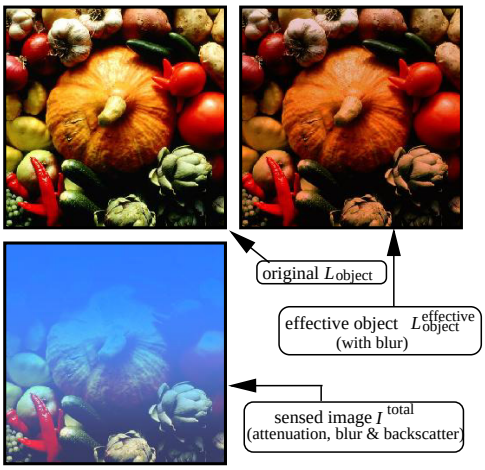

Figure 4. Simulating underwater imaging. The bottom part of the scene is set to be 0.5 meters away. The distance linearly changes to 3.5 meters at the top. We rendered the scene as if it is underwater, accounting for attenuation, blur (forward scattering) and backscatter. The latter effect is the prime cause for contrast degradation.

results are shown in Fig. 4. The effects of water are simulated using a model for oceanic water [21] with a low concentration of chlorophyll and a moderate concentration of hydrosols. Fig. 4 shows a colorful set of objects with radiance L_{object}. Then it shows $L_{\text{object}}^{\text{effective}}$, which accounts for blur by forward scattering. Note that the colors change a little due to forward scattering, since Eq. (4) includes an attenuation factor, which is implicitly wavelength dependent. We simulated the effects of varying distances by setting a distance map to the scene: the distance linearly increases from 0.5m at the bottom of the image to 3.5m at its top.

The visibility strongly deteriorates at the image I^{total}, which incorporates backscatter[3] and attenuation effects. Now, even objects at moderate distances are swamped in a veiling blue light and become obscured. Backscatter affects the color and contrast of even the close objects. This observation is consistent with analogous conclusions regarding visual degradation in the atmosphere: ambient light scattered into the LOS is the most important contributor to aerial image degradation [12], rather than blur [26]. It has also been observed in psychophysical studies [1] that human perception of an "atmosphere" is attributed to the additive contribution which we associate with backscatter. A similar conclusion applies underwater: backscatter is the dominant contributor to image degradation.

2.3 Polarization

Underwater scattering involves polarization effects. We exploit these effects to compensate for underwater visibility degradation, as we describe in the following sections. First, however, we describe the models for these effects. Consider a narrow source, which illuminates the scattering particles residing on the LOS. A *plane of incidence* is formed by a ray from the source to the LOS and by the LOS itself (Fig. 3). The backscattered light is partially polarized perpendicular to this plane. Recall that the natural illumination direction lies within a cone [6, 13] around the vertical axis (Fig. 2). For this reason, typically *underwater natural backscatter is partially polarized horizontally* [6, 13, 17, 35].

In order to sense the different polarization components we image the scene through a polarizing filter (Fig. 3). Since natural backscatter is partially polarized, then its intensity depends on the filter's orientation around the optical axis. There are two orthogonal orientations of the polarizer for which its transmittance of the backscattered light reaches extremum values $B^{\max}$ and $B^{\min}$. These are the two linear polarization components of the backscatter, i.e.,

$$B = B^{\max} + B^{\min} \quad , \tag{15}$$

where B is given by Eq. (12). The backscatter DOP is

$$p \equiv \left(B^{\max} - B^{\min}\right)/B \quad . \tag{16}$$

We assume that the effect of the signal S on the measured scene polarization is insignificant relative to the backscatter, since

1) Rough surfaces reflect depolarized light.

2) Polarization due to specular reflections is weaker [7] than in air. The reason is that the refraction index of water is closer to that of the reflecting material.

3) The signal polarization decreases as the distance to the camera increases. This is caused by multiple scattering along the LOS [22].

4) Even if the signal reaches the camera with substantial polarization, its influence is typically smaller than that of the backscatter. The reason is that the signal decreases (Eq. 7) while the backscatter (Eq. 12) increases with distance. Thus backscatter and the polarization of its electric field dominate the measurements as distance increases. Therefore, the validity of the assumption increases at distant objects, which are most affected by visibility degradation.

Nevertheless, note that this assumption may not hold at very close distances in a relatively good visibility, if the object strongly polarizes light as in [7, 27, 36].

3 Image Acquisition

When a polarizer is mounted, the sensed intensity at each image pixel changes as a cosine function of the filter orientation angle. Similarly to backscattered light, there are two orthogonal polarizer angles corresponding to extrema of the intensity, $I^{\max}$ and $I^{\min}$, where

$$I^{\text{total}} = I^{\max} + I^{\min} \quad , \tag{17}$$

while I^{total} is given by Eq. (14). Since we assume that the signal polarization is insignificant, the polarizer modulates

[3] The larger the object albedo, the stronger the signal is, relative to backscatter. Based on empirical studies of typical terrestrial objects [12], we set the average albedo to 0.2 .

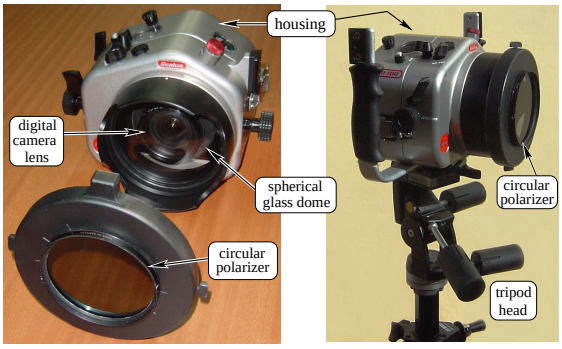

Figure 5. The Aqua-Polaricam. [Left] With the polarizer mount separated, the dome and lens are visible. [Right] The complete system mounted on a tripod.

only the backscatter. Therefore, the raw images corresponding to the extrema of the intensity measurements are

$$I^{\max} = S/2 + B^{\max} \quad \text{and} \quad I^{\min} = S/2 + B^{\min} \ . \quad (18)$$

Note that $I^{\min}$ is the image taken at the "best state" of the polarizer, where the disturbing backscatter is minimal [35]. On the other hand, $I^{\max}$ is the image taken at the "worst state" of the polarizer, where the backscatter is maximal.

In order to acquire such images we built a custom system for underwater polarimetric imaging, which we term the Aqua-Polaricam [16]. Several specifications determined its design, as described in the Appendix. Based on that, we built the system shown in Fig. 5. The housing is manufactured by Sealux and is commercially available. For the reasons explained in the Appendix, we close the housing with a *dome* port made of *glass*, while a *circular* polarizer is attached *externally* to it. The surrounding water flows to the space between the external polarizer and the dome, through several openings in the housing's interface to the polarizer mount. We use the Nikon D100 digital SLR camera, which allows for raw output data having a linear response (i.e., no gamma correction) without white balancing.[4]

We scuba-dived in Eilat (the Red-Sea) to a depth of 26 meters in an area containing coral reefs. We took images at the two states of the polarizer. The raw images have a very low contrast, as shown[5] in Fig. 6. Yet, their slight differences provide the key for substantial visibility improvement by a mathematical algorithm, described in Sec. 4.

3.1 Naive Attempt for Color Correction

As mentioned in Sec. 1, space-invariant enhancement methods do not model the spatially varying distance dependencies of visibility problems. Thus, they are of limited utility. As an example of a naive space-invariant enhancement,

[4] We verified the linear response of the system using different exposures of the MacBeth ColorChecker calibration chart.

[5] For clarity of display, the brightness of the displayed pictures in this paper underwent the same standard contrast enhancement (stretching), while their hue and color saturation were untouched. The recovery algorithms, of course, have used the raw (not brightness enhanced) images.

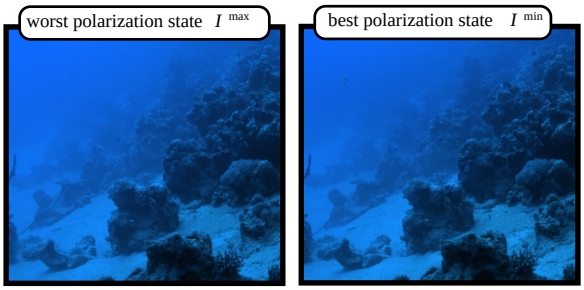

Figure 6. A scene 26m deep under the water surface. The images were taken using horizontal and vertical polarizer orientations. Both color images are contrast stretched, yet their visibility is poor. Their difference is hardly noticeable. **For high resolution *color* images, link to Ref. [29]**.

consider a simplistic method to compensate for the strong blue hue in any of the frames shown in Fig. 6. Recall that the images were taken in the water depths, where much of the red portion of the illumination spectrum had been absorbed by the water [34] while light had propagated down.

We know that the sand in the diving site shown in Fig. 6 is rather white. Suppose that we normalize the raw image color by the color of a sandy patch in the field of view. That multiplicative normalization does not compensate for the additive spatially varying backscatter. Hence the result does not perform a proper color compensation at varying distances, and certainly does not remove turbidity effects, as shown on the left part of Fig. 7.

4 Clear Underwater Visibility

Our algorithm for visibility recovery overcomes the "veiling" effect [4, 35] caused by backscatter. We thus use the adjective *unveiled* to describe the resulting image. After unveiling by compensation for the effects occurring along the LOS, we address the underwater illumination color bias.

Assume for a moment that we have an estimate of the global parameters B_∞ and p. From Eqs. (15,16,18), we estimate the backscatter as

$$\hat{B} = (I^{\max} - I^{\min})/p \ . \quad (19)$$

Inserting this estimate into Eqs. (12,14,17), we obtain an estimate for the "unveiled" object radiance

$$\hat{L}^{\text{effective}}_{\text{object}} = (I^{\text{total}} - \hat{B})/\hat{t} \quad \text{where} \quad \hat{t} = 1 - \hat{B}/B_\infty \ . \quad (20)$$

Here $\hat{t}$ is the estimated water transmittance, which is related to the object distance z by

$$\hat{t} = \exp(-\eta z) \ . \quad (21)$$

We process each color channel independently this way.

The unveiled image is an estimate of $L^{\text{effective}}_{\text{object}}$. We therefore do not compensate for image blur, but only for the veiling effect of backscatter and for attenuation. At this point we make do with this estimate. The reason stems from the discussion in Sec. 2.2: backscatter is the prime reason for image contrast degradation, hence overcoming backscatter,

rather than blur, is the prime step for recovering visibility. The unveiled image is a result of inversion of the image formation process. It therefore represents a recovery of the object, in contrast to methods which apply ad-hoc expressions of the DOP [4] for grayscale image enhancement.

To perform this recovery we need estimates of the global parameters B_∞ and p. These are intrinsic parameters of the water and lighting. This estimation is similar to methods which had been developed for open-air imaging [23]. We obtain these estimates by measuring pixels corresponding to objects "at infinity", i.e., which are so distant inside the water, that their signals are negligible due to attenuation.[6] After measuring p, we slightly increase it using the operation $p \rightarrow \epsilon p$, where $1 \leq \epsilon \leq 1/p$, before using p in Eqs. (19,20). According to Eqs. (19,20), this operation increases (biases) $\hat{t}$. Thus, it stabilizes the recovery at areas corresponding to very distant objects, where $t \rightarrow 0$. We used $\epsilon = 1.13$.

Compensating for the Illumination Color Imbalance

Eqs. (19-21) invert the spatially varying visibility degradation effects. This enables proper compensation for the color bias of the illumination. Similarly to Sec. 3.1, we use a patch of sand, which we know should be white, if it were not for the illumination color. Yet, contrary to Sec. 3.1, we perform the compensation using the recovered image $\hat{L}^{\text{effective}}_{\text{object}}$.

The result of the full scene recovery algorithm (unveiling and color compensation) is shown in the right part of Fig. 7. Compare this result to the left part of Fig. 7 in which no unveiling was attempted. Clearly, the recovered image has a much improved contrast and color. The ability to see objects in such hues under *natural* illumination at such an underwater depth is remarkable, considering the common knowledge [34]. The recovered image shows details unseen in the input images, and better shows the far objects. Results of recovering other underwater scenes are given in Ref. [29].

5 How Far Do We See?

We are interested in a *quantitative* estimate for the visibility improvement. A common criterion is the visibility range, i.e., the distance at which we may still observe certain details. Therefore, in this section we deal with the aspects of this criterion. As a by-product of the radiance recovery process, we get an estimate of the distance map of the scene. From Eq. (21) the distance z is estimated as a function of (x, y) up to a global scale factor η . It is given by

$$\widehat{\eta z}(x, y) = -\ln[1 - \hat{B}(x, y)/B_\infty] \qquad (22)$$

and shown in Fig. 8. We do not know what the attenuation coefficient η is. Nevertheless, we can quantitatively determine the *relative distances* in the scene. For example, when comparing two image regions, we can determine that one of them is, say, three times as distant from the camera as the other one. This indicates the ratio of improvement of the visibility range, which is achieved by the recovery method.

[6] The visibility range underwater is very short. Therefore, there are usually plenty of horizontal viewing directions in which no object is visible.

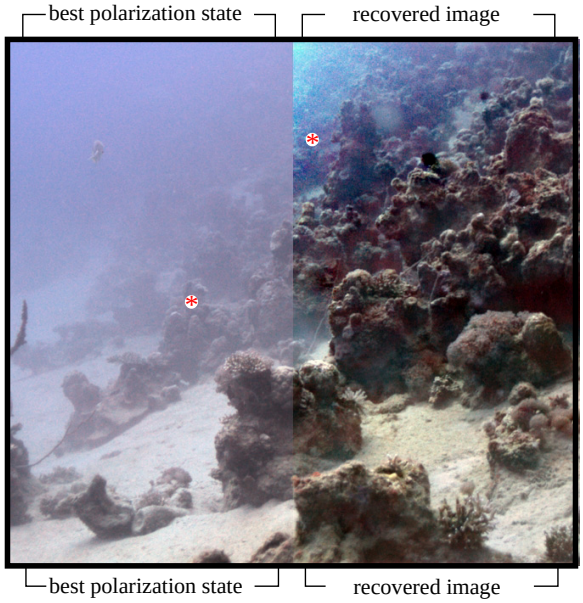

Figure 7. Comparison between the best raw image and the recovered image. These images underwent white balancing based on a white sand patch. In the raw image this process quickly loses its effectiveness as objects become more distant. In the unveiled image colors are recovered to large distances. **For high resolution color images, link to Ref. [29]**; The regions around the *marked points* have the same contrast in their respective images. However, the point in the recovered image part is twice as distant as the one in the raw image part, indicating the increase of visibility range.

To calculate the ratio of visibility ranges, we should compare the appearance of the same object at different distances. For a rough estimate, we selected from the scene two regions which have the following characteristics:

• Both regions have a similar object content.

• The contrast level of one region in the raw image, matches the contrast of the second region in the recovered image.

The selected pair of regions are around the marked points in Fig. 7. Both regions contain the same type of objects: chunks of the coral reef. We therefore assume that the intrinsic object properties are the same in these two regions.

The contrast of the marked left region in the raw image is the same as the contrast of the marked right region in the recovered image. To make this claim, we use a generalized definition of contrast at a region. Contrast between two points $v = 1, 2$ is usually defined by $|I_1 - I_2|/|I_1 + I_2|$, where I_v is the intensity at v. In a region having N pixels, we use

$$c = \text{STD}\{I_v\} / \left(\Sigma_{v=1}^{N} I_v\right) \quad , \qquad (23)$$

where $\text{STD}\{I_v\}$ is the standard deviation of the N intensity values. In order to minimize the contribution of noise, Eq. (23) was estimated only in the blue channel, for which

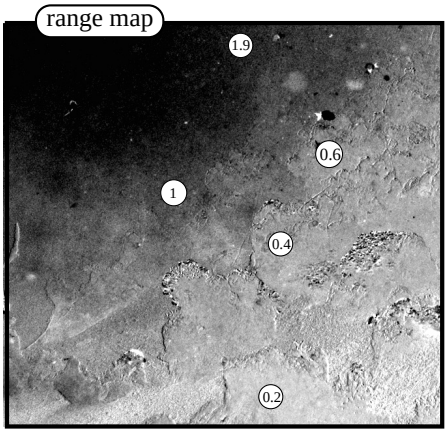

Figure 8. The estimated range map. Longer distances are displayed at darker graylevels. The distance to some points is written in units of the attenuation distance η^{-1}.

the signal to noise ratio is greatest.

To conclude, both regions have a similar object content. The contrast level of one region at a certain distance in the raw image matches the contrast of a farther region in the recovered image. Using Eq. (22), the range ratio between the points is 1.8. We therefore conclude that the method demonstrated an approximate doubling of the visibility range. We plan to follow up with more controlled experiments using standard calibration targets.

6 Conclusions

We presented an approach for overcoming degradation effects occurring in underwater vision. It is based on simple analysis of images acquired through a polarizer. The method is physics-based, hence it also recovers information about the scene structure (distances). We believe that it can lead to *useful* tools in underwater photography, underwater research, and underwater technological applications. See [29] for additional results and experiments.

Appendix : Building an Underwater Polaricam

As mentioned in Sec. 3, there are several specifications needed for the underwater imaging system. They arise since we make *quantitative* photometric measurements with the polarizer. The considerations are explained in detail in Ref. [16]. To make the current paper more self-contained, we briefly describe these issues here.

The camera should have a linear radiometric response and low noise. Its watertight housing should withstands the pressures in the depths at which we work. In addition, there should be full control of the camera parameters (exposure time, aperture, etc.). Therefore, the housing should couple to all the camera controls.

Optical Considerations

We use a polarizer to analyze the scene. However, we would like the *rest* of the optical system components to have *minimal effects* or sensitivities related to polarization. We achieve this by making the following decisions:

A dome port, or a flat port? The camera lens views the scene through a *port*, i.e., a transparent window in the housing [34]. Typical ports are flat or spherical. Suppose that we use a flat port. Then, consider the chief ray from an off-axis scene point. Since the chief ray is off axis, it is incident at an angle (i.e., not normal) to the flat port [16]. Therefore, at the interfaces of the port the transmittance depends on the polarization of the passing light [31]. This polarization dependence distorts the intensity readout values.

To alleviate this problem, we use a *dome port*. If the dome's center coincides with the center of projection of the camera, then the chief ray from an object point to the detector is normal to the dome interface. At normal incidence the transmittance is independent of polarization [31].

Minimizing photoelasticity consequences. Stress in the transparent port's material changes the polarization of the light it transmits. This effect is called the *photoelastic effect* [31]. Due to inhomogeneities in the material, this polarization effect is spatially varying. This spatially varies the transmittance though the polarizer [31], if the polarizer is placed inside the housing.

To alleviate this problem, we decided to place the polarizing filter *outside* the housing. The filter is thus the first optical component the light from the scene encounters as it enters the imaging system (See Fig. 5). The space between the polarizer and the dome is filled with water coming from the surroundings [16]. The photoelastic visible effects are indeed greatly diminished. Residual effects may persist, though. To further minimize them, we opted for a *glass dome*, since glass has a much smaller photoelasticity than polycarbonate materials (plastics) [31].

A circular or linear polarizer? In practice, the dome may not be precisely concentric with the center of projection. In non-normal incidence, different polarization components are differently transmitted by the port. To reduce this effect, we use a *circular polarizer*: it filters the linear polarization of its input (scene) while it outputs circular polarization [16, 31] to the dome. In this case, the dome transmittance is invariant to the polarizer angle. We note that circular polarizers are tuned to normal incidence and to a narrow spectral band. Light outside that band or off axis creates elliptical polarization. The port transmittance of elliptical polarization is still less variant to the polarizer angle, than when light is partially linearly polarized.

Acknowledgments

We are grateful to Nadav Shashar for helpful discussions. We are also grateful to Yoav Fhiler, Naftalli Blau and Nir Geva for their help in the diving. We wish to thank Yaakov Kahanov for supplying us with underwater archaeological pictures. Yoav Schechner is a Landau Fellow - supported

by the Taub Foundation, and an Alon Fellow. The work was supported by the Ollendorff Center in the Elect. Eng. Dept. at the Technion. Minerva is funded through the BMBF.

References

[1] E. H. Adelson, "Lightness perception and lightness illusions," in *The New Congitive Neuroscience* 2^{nd} ed., Ch. 24, 339-351 (MIT, Cambridge 2000).

[2] J. Åhlén and D. Sundgren, "Bottom reflectance influence on a color correction algorithm for underwater images," Proc. SCIA, 922-926 (2003).

[3] T. Boult, "DOVE: Dolphin omni-directional video equipment," Proc. Int. Conf. Robotics & Autom. 214-220 (2000).

[4] P. C. Y. Chang, J. C. Flitton, K.I. Hopcraft, E. Jakeman D. L. Jordan and J. G. Walker, "Improving visibility depth in passive underwater imaging by use of polarization,", App. Opt. **42**, 2794-802 (2003).

[5] F. Cozman and E. Krotkov, "Depth from scattering," Proc. CVPR, 801-806 (1997).

[6] T. W. Cronin and N. Shashar, "The linearly polarized field in clear, tropical marine waters: spatial and temporal variation of light intensity, degree or polarization and e-vector angle," J. Experim. Biol. **204**, 2461-2467 (2001).

[7] T. W. Cronin, N. Shashar, R. L. Caldwell, J. Marshall, A. G. Cheroske and T. H. Chiou "Polarization vision and its role in biological signalling," Integrative & Comperative Biol. **43** 549-558 (2003).

[8] L. J. Denes, M. Gottlieb, B. Kaminsky and P. Metes, "AOTF polarization difference imaging," Proc. SPIE **3584**, 106-115 (1998).

[9] H. Farid and E. H. Adelson, "Separating reflections and lighting using independent components analysis," Proc. CVPR, Vol. 1, 262-267 (1999).

[10] G. L. Foresti, "Visual inspection of sea bottom structures by an autonomous underwater vehicle," IEEE Trans. Syst. Man and Cyber, Part B **31**, 691-705 (2001).

[11] S. Harsdorf, R. Reuter and S. Tönebön, "Contrast-enhanced optical imaging of submersible targets," Proc. SPIE **3821**, 378-383 (1999).

[12] R. C. Henry, S. Mahadev, S. Urquijo and D. Chitwood, "Color perception throught atmospheric haze," JOSA A **17**, 831-835 (2000).

[13] G. Horváth and C. Varjú, "Underwater refraction-polarization patterns of skylight percieved by aquatic animals through Snell's window of the flat water surface," Vision Research **35**, 1651-1666 (1995).

[14] J. S. Jaffe, "Computer modeling and the design of optimal underwater imaging systems," IEEE J. Oceanic Engin. **15**, 101-111 (1990).

[15] Y. Kahanov and J. Royal, "Analysis of hull remains of the Dor D Vessel, Tantura Lagoon, Israel," Int. J. Nautical Archeology **30** 257-265 (2001).

[16] N. Karpel and Y. Y. Schechner, "Portable polarimetric underwater imaging system with a linear response," Proc. SPIE **5432** *Polarization: measurement, analysis and remote sensing VI* (2004).

[17] G. P. Können, *Polarized light in nature*, 1-10,96-99,131-137,144-145 (Cambridge University Press, 1985).

[18] J. M. Lavest, F. Guichard and C. Rousseau, "Multiview reconstruction combining underwater and air sensors," Proc. IEEE Int. Conf. Image Process. vol. 3, 813-816 (2002).

[19] M. Levoy, B. Chen, V. Vaish, M. Horowitz, I. McDowall and M. Bolas, "Synthetic aperture confocal imaging," Proc. SIGGRAPH (2004).

[20] B. L. McGlamery, "A computer model for underwater camera system," Proc. SPIE **208**, 221-231 (1979).

[21] C. D. Mobley, *Light and Water: Radiative Transfer in Natural Waters*, Ch. 3,5 (Academic Press, San-Diego 1994).

[22] S. P. Morgan, M. P. Khong and M. G. Somekh "Effects of polarization state and scatterer concentration on optical imaging through scattering media," App. Opt. **36**, 1560-1565 (1997).

[23] S. G. Narasimhan and S. K. Nayar "Vision and the atmosphere," Int. J. of Computer Vision **48**, 233-254 (2002).

[24] S. G. Narasimhan and S. K. Nayar "Contrast restoration of weather degraded images,", IEEE Trans. PAMI **25**, 713-724 (2003).

[25] S. K. Nayar, X. S. Fang and T. Boult, "Separation of reflection components using color and polarization," Int. J. Computer Vision **21**, 163-186 (1997).

[26] J. P. Oakley, "Improving image quality in poor visibility condiitons using a phusical model for contrast degredation," IEEE Tran. on Image Processing. **7**, 167-179 (1998).

[27] M. P. Rowe, E. N. Pugh Jr., J. S. Tyo, and N. Engheta, "Polarization-difference imaging: a biologically inspired technique for observation through scattering media," Optics Lett. **20**, 608-610 (1995).

[28] M. Saito, Y. Sato, K. Ikeuchi, and H. Kashiwagi, "Measurement of surface orientations of transparent objects by use of polarization in highlight," JOSA A **16**, 2286-2293 (1999).

[29] Y. Y. Schechner, *Home page*. Follow the link to *underwater imaging.* http://www.ee.technion.ac.il/∼ yoav/

[30] Y. Y. Schechner, J. Shamir and N. Kiryati, "Polarization and statistical analysis of scenes containing a semi-reflector," JOSA A **17**, 276-284 (2000).

[31] W. A. Shurcliff and S. S. Ballard, *Polarized light*, 98-103,120-121 (Van Nostrand Co., Princeton, 1964).

[32] J. S. Talyor, Jr., and L. B. Wolff "Partial polarization signature results from the field testing of the SHallow water Real-time IMaging Polarimeter (SHRIMP)," MTS/IEEE Oceans, Vol. 1, 107-116 (2001).

[33] K. J. Voss, "Simple emprical model of the oceanic point spread function," App. Opt. **30**, 2647-2651 (1991).

[34] M. Webster *The art and technique of underwater photography*, 19-22,33-39,146-149 (Fountain Press, Surray 1998).

[35] R. Wehner, "Polarization vision - a uniform sensory capacity?" J. Exp. Biol **204** 2589-2596 (2001).

[36] L. B. Wolff, "Polarization vision: a new sensory approach to image understanding," Image & Vision Comp. **15** 81-93 (1997).

[37] X. Xu and S. Negahdaripour, "Automatic optical station keeping and navigation of an ROV: sea trial experiment," Proc. Oceans, vol.1, 71-76 (1999).